Research Square

Preprints are preliminary reports that have not undergone peer review.
They should not be considered conclusive, used to inform clinical practice,
or referenced by the media as validated information.

Striatal inflammation is exacerbated by impaired resolution in a model of ASD: environmental enrichment rescues neuroimmune and behavioral deficits

Paola Bonsi

p.bonsi@hsantalucia.it

LIFE Institute for Research and Health Care - Santa Lucia IRCCS https://orcid.org/0000-0001-5940-9028

Martina Montanari
Marta Tiberi
Marc Dubourdeau
Giulia Ponterio
Maria Meringolo
Giulia Carrera
Francesco di Norscia
Francesca Balsamo
Ilham El Atiallah
Annalisa Tassone
Veronica Ceci
Stefano Saracini
Antonino Iurato La Rocca
Clara D'Ambra
Marta Ionta
Georgios Strimpakos
Francesca Gelfo
Valerio Chiurchiu

IRCCS Santa Lucia Foundation https://orcid.org/0000-0002-0316-7311

Article

Keywords:

Posted Date: July 31st, 2026

DOI: https://doi.org/10.21203/rs.3.rs-10535129/v1

License: This work is licensed under a Creative Commons Attribution 4.0 International License.
Read Full License

Additional Declarations: The authors have declared there is **NO** conflict of interest to disclose

Abstract

Autism spectrum disorder (ASD) is increasingly associated with neuroimmune dysregulation, yet the molecular mechanisms coupling synaptic dysfunction to circuit pathology remain unclear. Here we show that the ASD-associated R451C mutation in the Neuroligin-3 (*Nlgn3*) gene induces a neuroinflammatory process in the striatum, sustained by failure of the pathway of resolution of inflammation. Integrated lipidomic and cytokine profiling revealed a marked imbalance in the striatum of ASD mice, characterized by an increase in pro-inflammatory arachidonic acid–derived eicosanoids and depletion of specialized pro-resolving mediators and their DHA/EPA precursors. The lipidomic dysregulation was accompanied by increased pro-inflammatory cytokines as well as defective anti-inflammatory counter-regulation. High-dimensional immunophenotyping uncovered a persistent shift of striatal microglia toward a pro-inflammatory, antigen-presenting state and a concomitant bias toward neurotoxic-like astrocytes. Importantly, eight weeks of environmental enrichment fully normalized lipid and cytokine signatures, and restored homeostatic glial phenotypes. Notably, the prolonged stimulation also rescued the corticostriatal synaptic plasticity deficits, and reversed social, motivational, repetitive, and motor abnormalities of R451C-*Nlgn3* mice. These findings suggest a defective regulation of the inflammation-resolution balance as a mechanistic bridge between ASD-linked postsynaptic gene mutations and circuit dysfunction and demonstrate that environmental enrichment can re-engage endogenous resolution pathways and restore striatal function and behavior.

Introduction

Autism spectrum disorder (ASD) is a neurodevelopmental condition characterized by persistent deficits in social communication and interaction, as well as restricted, repetitive patterns of behavior, interests, or activities (1). Although substantial progress has been made in identifying genetic contributors to ASD, including rare high-penetrance mutations affecting synaptic function, these variants alone cannot fully account for the complexity and variability of the disorder (2). Converging evidence now indicates that ASD emerges from dynamic interactions between genetic risk factors and environmental conditions that together shape early brain development (3). Among the biological systems, the neuroimmune network, which plays essential roles in synaptic refinement, circuit maturation, and maintenance of neural homeostasis, is highly sensitive to such an interaction (4–6).

Over the past decade, neuroimmune dysregulation has gained increasing attention in ASD. Postmortem and clinical studies consistently revealed altered cytokine signatures, aberrant microglial activation states, and chronic low-grade inflammation in children and adults with ASD (7–9). Functional neuroimaging and transcriptomic data further suggest that these immune alterations are not merely secondary consequences but may contribute directly to atypical circuit development and behavioral trajectories. While pro-inflammatory signaling has been the primary focus of most studies on neuroimmune dysfunction in ASD and related neurodevelopmental disorders, recent work on the biology of inflammation indicates that termination of the immune responses and restoration of tissue homeostasis is an active process, mediated by a specific resolution pathway. This phase is mediated by

specialized pro-resolving lipid mediators (SPMs) (10, 11), regulatory cytokines, and homeostatic glial programs (12–14). Failure of resolution, observed in several neuropsychiatric and neurodegenerative conditions, can sustain maladaptive inflammatory states long after the initial trigger, thereby perturbing circuit function during key time-windows of development (15–17).

Environmental factors, including stress, diet, and sensory stimulation, are known modulators of immune function and can strongly influence both inflammatory and resolution pathways (18–22). In the context of ASD, these environmental influences may exacerbate or mitigate neuroimmune vulnerabilities conferred by genetic risk (23–27). This concept raises the possibility that targeted environmental interventions could normalize pathological immune signatures and thereby restore the conditions necessary for healthy circuit maturation. Environmental Enrichment (EE), an experimental paradigm that enhances sensory, cognitive, and social stimulation, has been shown to promote synaptic plasticity, remodel glial states, and regulate peripheral and central immune signaling in experimental models (28–33). Yet, despite substantial interest in the protective and therapeutic potential of EE, its ability to correct genetically driven neuroimmune abnormalities and restore impaired resolution programs in ASD models remains insufficiently explored.

Here, we address this gap by investigating the impact on neuroimmune function of mice with the ASD-associated R451C mutation in the Neuroligin-3 (*Nlgn3*) gene, encoding a postsynaptic adhesion molecule implicated in synaptic transmission (34, 35), and the ability of EE to rescue these alterations, as well as previously described circuit and behavioral dysfunctions (36–38).

We report a significant imbalance between the pro- and anti-inflammatory pathways in the striatum of the R451C-*Nlgn3* mouse model. Notably, we found that EE is able both to restore a correct neuroimmune balance, and to rescue the profound alterations in corticostriatal function and ASD-relevant behaviors previously reported in R451C-*Nlgn3* mice.

Materials and methods

Experimental model

For the present study, adult (postnatal days 60–90) male R451C-*Nlgn3* (KI) mice (B6;129-Nlgn3tm1Sud/J) and their wild-type (WT) littermates were utilized. All the procedures were approved by IRCCS Fondazione Santa Lucia ethics committee, and authorized by the Italian Ministry of Health (nr. 739/2022-PR), in accordance with the European Union Directive 2010/63/EU and Italian D. Lgs 26/2014. For genotyping, the R451C mutation was detected by PCR amplification of the insertion site of the first loxP site in the *Nlgn3* gene (forward 5'-TGTACCAGGAATGGGAAGCAG-3'; reverse 5'-GGTCAGAGCTGTCATTGTCAC-3') from genomic DNA extracted from the mouse tail, as previously described (36–38).

Targeted-metabololipidomics analysis of lipid mediators

Striatal samples from KI and WT mice were fast frozen and stored at -80°C for a maximum of 6 months before lipidomic analysis to prevent alteration of lipid content. Fifty-four oxylipins and metabolites of AA, EPA and DHA were quantified using very sensitive and selective targeted liquid chromatography coupled to tandem mass spectrometry (LC-MS/MS). Lipid mediators were extracted by solid-phase extraction (SPE) and eluted with a mixture of methyl-formate and methanol (MeOH). After solvent evaporation, samples were dissolved in MeOH:H2O, 50:50 (v/v) and injected into an ultra-high-performance liquid chromatography U-HPLC Exion LCAD system coupled to a 6500 + QTRAP (AB SCIEX GmbH, Zug, Switzerland) mass spectrometer. The lipids were separated on a Kinetex C18 column (100 x 2.1 mm; 1.7 µm, Phenomenex) and detected in negative electrospray ionization using multiple reaction monitoring (MRM) mode. When authentic standards were available, the identification of the lipid mediators in the samples was based on matching of their retention time with the retention time of the pure standards injected in the same conditions. Calibration curves were obtained using the same authentic standards, and quantification was carried out based on peak areas from multiple reaction monitoring (MRM) transitions using a linear model weighted by 1/X (X, the nominal concentration). For 21-HDOHE, 4(S),14(S)-DiHDOHE, RvD6, 18(S)- RvE3, 18(R)-RvE3 identification was based solely on theoretical MRM transitions established on the basis of the molecule's structure, and quantification was carried out using a pure standard with a similar structure. Peak detection, integration, and quantitative analysis were performed using Sciex OS MQ software (39, 40). Quantification results expressed in pg/mL are reported in Supplementary Table 1.

Dissociation of brain areas

After animal sacrifice, the striatum and hippocampus were collected and immersed in D-PBS with high glucose buffer at 4°C. According to the manufacturer’s protocol, tissues were immediately dissociated to single-cell suspension by enzymatic degradation and myelin removal using the adult brain dissociation kit and GentleMACS dissociator (Miltenyi Biotec). The isolated tissues were placed in C-tubes, and a mix containing Enzyme P and Buffer Z was added to the samples. A second mix containing Enzyme A and Buffer Y is then added, C-tubes tightly closed and attached upside down onto the sleeve of the gentle MACS Octo Dissociator with Heaters (Miltenyi Biotec). The appropriate program 37C_ABDK_02 was run for 30 minutes, c-tube was detached and centrifuged to collect the sample, which was then resuspended and filtered to a 70 um MACS SmartStrainer with 10 ml of cold D-PBS with high glucose. After centrifugation at 300g for 10 minutes, the sample was resuspended in the debris removal solution, gently overlayed in cold D-PBS with high glucose, and centrifuged at 3000g for 10 minutes with full acceleration brake. The two top phases were aspirated and discarded, and the sample was resuspended in cold D-PBS with high glucose, centrifuged at 1000g for 10 minutes, and then resuspended in a staining buffer ready for cell count and flow cytometry staining (41–43).

Immunophenotyping by high-dimensional flow cytometry

Cellular phenotypes were evaluated using multiparametric flow cytometry panels containing markers to identify cell types and activation states (41–43). These markers allowed us to limit the analysis to the cells of interest, based on physical parameters (side and forward scatter) (Supplementary Fig. 1). For striatum and hippocampus immunophenotyping, cells in suspension were stained at the surface or intracellularly with two different panels for 15 minutes at 4°C in the dark. After staining, cells were washed and resuspended in PBS. Briefly, cells were first gated as CD45 + to identify the total leucocytes/resident immune cells; within this gate, microglial cells were identified as $CD45^{low}CD11b/c^{+}$ cells. Within microglial cells, the expression of pro-inflammatory (CD80/86, MHC-II, CD68 and iNOS) and anti-inflammatory/pro-resolving markers (CD206, CD200R, CD163, Trem2) were evaluated. Astrocytes were identified as ACSA-2 + cells and the expression of C3 and S100A10 was further assessed within the astrocyte cell population. All samples were analyzed on a 13-color Cytoflex (Beckman Coulter). For each analysis, at least 0.2×10^{6} live cells were analyzed by gating on Aqua Live/Dead negative cells and then analyzed using the Flowjo analysis software (FlowJo 10.0); Tre Star; https://www.flowjo.com/solutions/flowjo).

ELISA assays

The levels of cytokines/chemokines in striatal homogenate were measured by standard sandwich ELISA through custom-made magnetic Luminex multiple assays (R&D Systems), according to the manufacturer's instructions, and read on a Luminex200 (Life Technologies) (44).

Environmental enrichment

At weaning (postnatal day 30), balanced groups of WT and R451C-*Nlgn3* littermates were housed in groups in either No Enrichment (NE), or Environmental Enrichment (EE) condition for eight weeks.

NE

mice were housed in groups of 4 balanced by genotype in standard mouse cages (15 cm x 37 cm x 13 cm) with bedding, a transparent red triangle plastic Mouse House™, nesting tissue paper, and *ad libitum* food and water. Cages were cleaned once a week.

EE

mice were housed in groups of 12, balanced by genotype, in larger, two-story cages (GR1800 Double Decker for rats, Tecniplast) containing a ladder, a steel ring, and two wheels for motor stimulation, as well as diverse social, sensory and cognitive stimuli, provided by a combination of eight objects of different material (plastic, wood, steel, and glass), size, shape, and color (28–31, 45–47). The objects included two nesting materials (paper wool, sizzle nest, or wood wool), two tiny houses that allow mice to take refuge (tubes, igloo, hut or burrows) and a different combination of four objects (a spinning top, marbles, a rock, a ball, construction bricks and pieces, or dumbbells) that were replaced once a week.

Behavioral tests

Twelve-week-old mice were used for behavioral analyses, performed as previously described (36–38), and detailed below. Animals were tested between 8 AM and 4 PM, on different days, after handling habituation. To explore behaviors of the ASD mouse model, we utilized the Research Domain Criteria (RDoC) framework, which aims at establishing an experimental categorization system where symptoms/domains are classified by anchoring them to the etiological and pathophysiological evidence (https://www.nimh.nih.gov/research/research-funded-by-nimh/rdoc/index.shtml).

Three-chamber social interaction test

The 3-chamber test was used to study sociability and social novelty. The apparatus consisted of a rectangular plexiglass box (60 x 40 x 22 cm). One hour prior to the test, animals underwent isolation and acclimatization to the apparatus. The experimental procedure involved three 10-minutes-phases: habituation (mice freely explore the chambers), sociability (mice explore an inanimate object or a stranger mouse) and social novelty phase (mice interact with a familiar mouse or a novel stranger mouse). Interaction was defined as the test mouse's nose being within 2 cm of the wire cup as previously described (36–38). Each session was video-recorded and analyzed using Ethovision XT 16. Two indices were used: the Sociability Index (preference for a conspecific (S) with respect to an object (O)) is measured by the percentage of time spent in close interaction with either S or O on the total time spent interacting with S and with O and the Social Novelty index (preference for the novel (N) with respect to the familiar (F) conspecific), expressed as the percentage of time spent in close interaction with either N or F on the total time spent interacting with N and with F (48).

Sucrose splash test

The Sucrose Splash Test was performed for investigating anhedonia and motivational behavior. Mice were placed in a standard plexiglass cage (15 x 30 x 20 cm) and sprayed twice with a 10% sucrose solution onto the dorsal fur. The delay before initiation and the total duration of the grooming behavior were recorded over a 5-minute period using video recording (49).

Marble burying test

Mice were individually housed in a polycarbonate cage measuring 26 x 48 x 20 cm, filled with 5 cm clean bedding. Twenty marbles were tidily laid in four rows on the surface of the bedding that was photographed at 5-minute intervals during the 30-minute-long test, to better quantify the number of buried marbles (50, 51).

Repetitive self-grooming

During spontaneous open-field activity, we additionally examined the self-grooming behavior, scoring the total number of grooming episodes, defined as complete sequences of cleaning and rubbing the face

and snout, licking and stroking flanks and abdomen, ano-genitals and tail (36–38).

Open field test

This test specifically focused on the normalized distance traveled by mice in the arena central area, defined as a zone 5 cm away from the walls. Data acquisition and analysis were performed using Ethovision XT 16. Following the experimental procedure, a comprehensive analysis was conducted on a range of behavioral parameters (36–38).

Accelerated rotarod test

The rotarod test was performed using an electronically controlled computerized system (Panlab, Harvard Apparatus), which consists of a rotating cylinder with four lanes (3 cm diameter). Each session consisted of 3 trials at 5-minute intervals. The latency to fall (seconds) was measured (36–38).

Y-maze test

The apparatus was in white acrylic plastic, with three identical arms measuring 8x30x15 cm, set 120° apart. Each trial lasted 10 minutes, and was recorded and analyzed using Ethovision XT 16. Spatial working memory performance was quantified by calculating the alternation percentage of triads (ABC, BCA, CAB) over the total number of arm entries (36–38).

Slice preparation and electrophysiology recordings

Male mice were euthanized by cervical dislocation. Corticostriatal coronal slices (220 µm) were cut with a vibratome in Krebs' solution, bubbled with 95% O2 and 5% CO2, as previously described (36–38). Slices were transferred into a recording chamber (0.5-1 ml volume), perfused with oxygenated Krebs' solution at constant temperature (32–33°C) and flow rate (2–3 ml/min).

Striatal projection neurons (SPNs) were visualized using BX51WI microscopes (Olympus), with differential interference contrast (IR-DIC) and standard infrared optics, and identified based on their morphology and electrophysiological properties. Electrophysiological signals were detected using Multiclamp 700B amplifiers coupled to pClamp 10.6 software (Molecular Devices). Data analysis was performed offline using Clampfit 10 (Molecular Devices)Voltage- and current-clamp recordings were performed with borosilicate glass pipettes (resistance 5–10 MΩ) filled with an internal solution containing (in mM): 125 K+ - gluconate, 10 NaCl, 1 CaCl2, 2 MgCl2, 0.1 BAPTA, 19 HEPES, 0.3 Na-GTP, 2 Mg-ATP; pH 7.35; 300 mOsm. For - (S)-3,5-dihydroxyphenylglycine-induced long-term depression (DHPG-LTD) experiments, SPNs were clamped at -50 mV holding potential, and excitatory postsynaptic currents (EPSCs) evoked using bipolar electrodes, in the presence of 50 µM picrotoxin (PTX, Sigma-Aldrich), as previously described (36–38).

Statistical analysis

Statistical analysis was performed using Prism software v.10 (GraphPad). Based on Shapiro-Wilk test's assessment of data distribution normality, a Student's t-test was used for comparisons between 2

groups. Two-way ANOVA, followed by Bonferroni's multiple comparisons test, was utilized to analyze ≥ 3 groups of data with normal distribution.

Results

An integrated lipid and cytokine profiling reveals an altered inflammation-resolution interplay in the R451C- Nlgn3 striatum.

Previous work indicated substantial synaptic alterations in the striatum of the R451C-*Nlgn3* mouse model of ASD (36–38). To investigate a possible neuroimmune contribution to the molecular mechanisms underlying these alterations, we performed an integrated LC-MS/MS–based lipidomic characterization of pro-inflammatory and pro-resolving lipid mediators in striatal samples of R451C-*Nlgn3* KI mice and their WT littermates (Fig. 1A). The R451C mutation produced a clear imbalance between inflammatory and inflammation-resolving lipid species. In particular, pro-inflammatory eicosanoids, including multiple prostaglandins (PGs) and related arachidonic acid derivatives, were elevated in mutant mouse tissue (Fig. 1B-D), indicating an increased drive toward inflammatory activation. However, the lipid families responsible for terminating inflammation, namely specialized pro-resolving mediators (SPMs), including lipoxins (LXs), resolvins (RvDs and RvEs), and maresins (MaRs), were consistently diminished (Fig. 1B,C,F), together with their DHA- and EPA-derived biosynthetic precursors (Fig. 1B,C,E). This pattern unveils an intrinsic failure to engage the lipid-based pathways required to extinguish inflammatory signaling in the striatum. This hypothesis was corroborated at the cytokine/chemokine level, whereby striatal homogenates from R451C-*Nlgn3* mice exhibited elevated concentrations of pro-inflammatory mediators, including IL-1β, IL-6, TNF-α, IFN-γ and CCL3, whereas ICAM-1 or the anti-inflammatory cytokines IL-10, IL-4, and CCL4 were unchanged or undetectable (Fig. 1G), further supporting the occurrence of a heightened inflammatory state coupled with failure of an effective counterbalance regulatory response within the striatal microenvironment.

Together these findings converge to indicate that the R451C mutation in the *Nlgn3* gene induces a dual disruption of neuroimmune homeostasis, characterized by an enhanced inflammatory drive coupled with defective resolution, providing evidence of a significant impact of an ASD-linked synaptic gene mutation on the neuroimmune system.

Immunophenotypic shifts in striatal microglia of R451C- Nlgn3 mice

We next assessed the glial activation state, to evaluate whether the neuroimmune disturbances observed in the striatum of the R451C-*Nlgn3* model can be ascribed to a phenotypic shift in the microglial and/or astrocyte populations. High dimensional flow cytometry (Fig. 2A, Supplementary Fig. 1) of $CD11b^{+}CD45^{+}$cells revealed a pronounced shift in the microglial phenotype of R451C-*Nlgn3* striatum. In particular, KI microglia displayed elevated expression of classic activation markers, including the co-stimulatory receptors CD80/CD86, the antigen presenting MHC-II, the phagolysosomal protein CD68, and the inducible enzyme iNOS (Fig. 2B), indicating a bias toward a pro-inflammatory, neurotoxic activation state compared with WT littermates. Concomitantly, mutant mice microglia showed reduced

surface levels of the anti-inflammatory markers CD206, CD200R, CD163, and TREM2 (Fig. 2C), consistent with a shift from homeostatic or reparative phenotypes toward profiles linked to impaired resolution of inflammation. These findings were corroborated by our observations in the astrocytic compartment, indicating that glial reactivity in the R451C striatum is not exclusively confined to microglia. Indeed, analysis of ACSA-2^{+}cells showed that astrocytes from KI mice exhibited increased expression of C3, a hallmark of neurotoxic A1 astrocytes, whereas the A2-associated marker S100A10 remained unchanged, indicating that the observed A1-like shift is not counterbalanced by induction of a more protective A2-like program (Fig. 2D). This astrocytic immunophenotype therefore converges with the microglial profile to support a maladaptive, pro-inflammatory glial network within the R451C striatum. Notably, these glial alterations were not observed in the hippocampus, either for microglial M1/M2-like markers (Supplementary Fig. 2A,B) or for astrocyte activation markers (Supplementary Fig. 2C), highlighting a regional specificity of the R451C-*Nlgn3*-induced neuroinflammatory remodeling.

Together with lipid and cytokine signatures, this integrated immunoprofiling delineates a coherent scenario in which the R451C mutation locks striatal microglia into a persistently pro-inflammatory, poorly resolving state, providing a cellular substrate through which ASD-linked synaptic mutations can drive chronic neuroimmune dysregulation in circuits governing social and repetitive behaviors.

Environmental enrichment reverses inflammatory and neuroimmune alterations

Given the pronounced pro-inflammatory bias and impaired resolution tone characterizing the R451C-*Nlgn3* striatum, we next asked whether Environmental Enrichment (EE) could restore neuroimmune homeostasis. To this aim, R451C-*Nlgn3* and WT littermates were reared for eight weeks in either standard non-enriched (NE) or EE conditions before undergoing neuroimmune evaluations. EE markedly reduced the expression of canonical pro-inflammatory microglial markers that were elevated in KI mice reared in standard conditions (Fig. 3A), indicating a recovery from the neurotoxic, antigen-presenting phenotype. In parallel, EE restored microglial homeostatic and anti-inflammatory markers (Fig. 3B). Astrocytic reactivity was similarly corrected, whereby EE significantly suppressed C3, while enhancing S100A10 level (Fig. 3C), indicating a drift from neurotoxic A1 reactivity toward a homeostatic A2 phenotype. At the cytokine level, EE abolished the enhanced pro-inflammatory cytokine production, observed in the striatum of KI mice reared in standard conditions, with a significant rescue effect on IL-6 and TNF-α, while modestly increasing the anti-inflammatory cytokine IL-10 (Fig. 3D).

Overall, together with the restoration of anti-inflammatory and homeostatic glial markers, these changes indicate that EE reinstates the molecular conditions necessary for the resolution of inflammation.

Environmental enrichment reverses the behavioral alterations and restores corticostriatal synaptic plasticity

Since EE was able to normalize the inflammatory and glial landscape of the R451C-*Nlgn3* striatum, we next asked whether the rescue of the neuroimmune microenvironment was accompanied by improvements in the behavioral and synaptic phenotypes that characterize KI mice (36–38). To this aim, we first investigated the expression of corticostriatal long-term synaptic plasticity. As previously reported, striatal projection neurons (SPNs) recorded from R451C-*Nlgn3* mice do not express long-term depression (LTD) of corticostriatal synaptic transmission in response to either high-frequency stimulation (HFS-LTD) or group I metabotropic receptors activation with (RS)-3,5-dihydroxyphenylglycine (DHPG-LTD) (36–38). The 8-week-long EE treatment did not modify either SPN membrane properties (data not shown), or the kinetics of excitatory postsynaptic currents (EPSCs) (Supplementary Fig. 3E,F). Notably, however, DHPG-LTD at corticostriatal synapses of KI mice was fully restored by EE treatment (Fig. 4G,H).

Similarly, EE exerted a broad rescuing effect across social, motivational, and repetitive behavioral domains. In the three-chamber test, KI mice housed in the EE condition showed fully restored sociability (Fig. 4A) and social novelty preference (Fig. 4B), performing indistinguishably from WT littermates. The recovery of social behavior paralleled improvements in the motivational drive in the splash test, where EE-reared KI mice showed a rescue of self-care grooming activity, indicating a reversal of the motivational blunting observed in standard housing conditions (Fig. 4C). EE also corrected repetitive and stereotyped behaviors, measured in the marble burying test (50, 51), where KI mice reared in the EE condition displayed a significant reduction both in the number of marbles buried (Fig. 4D,E), as well as in the duration of grooming during spontaneous exploration (Fig. 4F). Hyperactivity and increased exploratory drive, which were prominent in KI mice in the open field and Y-maze tests, were similarly corrected by EE, without altering spontaneous alternation rates (Supplementary Fig. 3A-C), suggesting a selective modulation of arousal and motivational circuits rather than hippocampus-dependent working memory. The superior motor performance of KI with respect to WT littermates in the accelerating rotarod test, ascribed to an excessive consolidation of repetitive motor routines in R451C-*Nlgn3* mice (36, 38), was also normalized by EE treatment (Supplementary Fig. 3D).

Together, these findings show that EE can rescue behavioral activity, as well as striatal neuroimmune and synaptic function, in R451C-*Nlgn3* mice.

Discussion

Numerous ASD-associated genetic variants, among which the R451C substitution in the *Nlgn3* gene, disrupt synaptic adhesion and transmission, directly impacting neuronal circuit function (52). Indeed, previous work reported synaptic deficits in diverse brain regions and animal models of ASD, and particularly in the striatum of R451C-*Nlgn3* KI mice (36–38). Further evidence, however, drew attention to the role of neuroimmune dysregulation in the pathogenesis of ASD (26, 53, 54). Several ASD-associated genes encode components of the immune system, and studies on postmortem tissue and human iPSC-derived models, as well as imaging data from patients, consistently documented microglial activation, cytokine elevations, and glial reactivity (6, 55–58). This neuroimmune profile parallels the peripheral and

CSF perturbations reported in ASD patients, in particular a correlation of IL-6 and TNF-α levels with symptom severity, and a significantly weakened IL-10, IL-4 anti-inflammatory pathway (59–61).

Neuroimmune imbalances have been reported also in experimental models of ASD (4, 62). In particular, alterations in morphology and cell density of microglia and astrocytes were described in the hippocampus of R451C-*Nlgn3* mice, suggesting subtle functional changes that may precede a reactive state (57). These observations are in line with the lack of an overtly reactive phenotype in our high dimensional flow cytometry analyses of $CD11b^{+}CD45^{+}$ and $ACSA\text{-}2^{+}$ glial cells, as well as in the levels of pro-inflammatory cytokines in the hippocampus of KI mice. Conversely, in accordance with the observations in patients, in the striatum of R451C-*Nlgn3* mice we observed a pronounced shift of microglia and astroglia toward a neurotoxic phenotype, together with increased concentrations of pro-inflammatory cytokines. These observations are consistent with converging evidence implicating cortico-striatal and mesolimbic circuits in ASD-relevant behavioral domains, including reward-related motivation, repetitive/habit-like behaviors, and social processing, both in patients and animal models (38, 63–67).

Importantly, the pro-inflammatory signatures detected in the striatum of R451C-*Nlgn3* mice are accompanied by concomitant lack of activation in the pro-resolving pathway. To our knowledge, this is the first report of a failure of the inflammation resolution system in a genetic model of ASD. This observation has noteworthy implications. Inflammation is a physiological process that is beneficial when circumscribed in time and space, but detrimental when it overcomes tightly regulated limits, which are imposed by the pro-resolving pathway. Therefore, failure of the latter allows an indiscriminate continuation of inflammation, causing damage over time. An uncontrolled inflammatory drive provides a molecular scaffold for synaptic instability, as SPMs not only quench cytokines, but also safeguard synaptic integrity through glial reprogramming, a process proven deficient in maternal immune activation models of ASD (55, 56).

To further investigate the imbalance between pro-inflammatory and pro-resolving pathways, we performed a lipidomic analysis and revealed, for the first time in an ASD model, an additional signature of unresolved inflammation, whereby upregulated arachidonic acid-derived prostaglandins parallel depleted SPMs and their DHA/EPA precursors. These findings mirror SPM defects reported in diverse neurological conditions, including Alzheimer's disease and schizophrenia, where SPM supplementation mitigates pathology (68–70). In the R451C-*Nlgn3* striatum, SPM depletion might sustain the pro-inflammatory lipid/cytokine phenotype and glial priming, which, in turn, may amplify synaptic instability during postnatal periods of synaptic pruning (71). In turn, glial alterations likely contribute to the synaptic and circuit dysfunctions that determine social avoidance, repetitive behaviors and stereotypies, and motivational blunting in R451C-*Nlgn3* mice. Hence, our findings suggest a convergence between postsynaptic adhesion defects and glial/neuroimmune maladaptations, which, together with synaptic and corticostriatal circuit abnormalities, may collectively contribute to the ASD-like behavioral abnormalities observed in R451C-*Nlgn3* mice (36–38, 61, 63).

Notably, the 8-week-long EE treatment reversed all the alterations observed in the KI mouse striatum, rescuing the inflamed milieu and the pro-inflammatory glial phenotype, restoring synaptic plasticity, and recovering mouse behaviors. These observations are in line with the established roles of EE in enhancing BDNF, neurogenesis, and peripheral immune regulation (72–74). Interestingly, the present data suggest that the effects of EE may extend also to central SPM and glia, possibly via upregulation of lipoxygenase pathways or dampening of TLR signaling in microglia induced by sensory-motor stimulation (75).

These findings can also inform on the gene-environment interplay in ASD, whereby they show that early EE-mediated activation of endogenous resolution pathways can revert the predisposition of the neuroimmune system to fragility caused by mutation in a postsynaptic adhesion gene.

Further studies are needed to clarify whether such intervention could be effective also if applied later along postnatal development.

In a translational viewpoint, these observations suggest that peripheral SPM/cytokines might be identified as biomarkers useful to stratify patients for personalized medicine, using either potentially disease-modifying EE interventions, such as sensory-integration therapies or augmented environments, or pharmacological therapies with SPM mimetics.

Declarations

Conflict of interest

The authors declare no competing interests.

Author Contributions

MMo, GP, MMe, AILR, CDA, MI: Animal handling, behavioral experiments, data analysis; MT, GC, VCe, SS: Flow cytometry immunophenotyping; MD: Lipidomic analysis; MMo, GP, IEA, AT: electrophysiology, data analysis; FB: Environmental enrichment; MMo, GP, VCe, GC: ELISA assays; FDN: Bioinformatic analyses; GS: Animal model; FG: Environmental enrichment design and supervision; MMo, VCh, PB: .Data analysis and interpretation, study planning, manuscript writing; VCh, PB: Study conceptualization, research supervision, manuscript revision, financial support. All authors reviewed, edited, and approved the final manuscript.

Acknowledgements

This work was supported by an Autism Research Institute 2022 Research Grant to P.B. and V.Ch.. The research was also partly supported by "Fondi Ricerca Corrente 2026" of the Italian Ministry of Health. The authors wish to thank Dr. Eugenia Landolfo for kind support in the environmental enrichment model

handling, and Dr. Annarita Wirz, Mr. Alessio Fieramosca, Mr. Massimiliano Di Virgilio, and Mr. Gianni Cantini for support and assistance with animal care.

References

1. American Psychiatric Association. Diagnostic and statistical manual of mental disorders. American Psychiatric Association Publishing; 2022.
2. Bourgeron T. From the genetic architecture to synaptic plasticity in autism spectrum disorder. Nat Rev Neurosci. 2015;16(9):551–63.
3. Quiñones-Medina E, Galleguillos F, Parra V, Arriagada G, Bustos FJ. Gene-Environment Interactions in Autism Spectrum Disorders: The Role of Bisphenol A in Modulating Genetic Susceptibility. Autism Res. 2026;
4. Matta SM, Hill-Yardin EL, Crack PJ. The influence of neuroinflammation in Autism Spectrum Disorder. Brain Behav Immun. 2019;79:75–90.
5. Liao X, Yang J, Wang H, Li Y. Microglia mediated neuroinflammation in autism spectrum disorder. J Psychiatr Res. 2020;130:167–76.
6. Liao X, Liu Y, Fu X, Li Y. Postmortem studies of neuroinflammation in autism spectrum disorder: a systematic review. Mol Neurobiol. 2020;57(8):3424–38.
7. Hughes HK, R J Moreno, Ashwood P. Innate immune dysfunction and neuroinflammation in autism spectrum disorder (ASD). Brain Behav Immun. 2023;108:245–54.
8. Toscano CVA, Barros L, Lima AB, Nunes T, Carvalho HM, Gaspar JM. Neuroinflammation in autism spectrum disorders: Exercise as a “pharmacological” tool. Neurosci Biobehav Rev. 2021;129:63–74.
9. Frasch MG, Yoon B-J, Helbing DL, Snir G, Antonelli MC, Bauer R. Autism Spectrum Disorder: A Neuro-Immunometabolic Hypothesis of the Developmental Origins. Biology (Basel). 2023;12(7).
10. Serhan CN, Chiang N, Dalli J. The resolution code of acute inflammation: Novel pro-resolving lipid mediators in resolution. Semin Immunol. 2015;27(3):200–15.
11. Buckley CD, Gilroy DW, Serhan CN. Proresolving lipid mediators and mechanisms in the resolution of acute inflammation. Immunity. 2014;40(3):315–27.
12. Butovsky O, Weiner HL. Microglial signatures and their role in health and disease. Nat Rev Neurosci. 2018;19(10):622–35.
13. Sanjabi S, Oh SA, Li MO. Regulation of the Immune Response by TGF-β: From Conception to Autoimmunity and Infection. Cold Spring Harb Perspect Biol. 2017;9(6).
14. Ogawa Y, Duru EA, Ameredes BT. Role of IL-10 in the resolution of airway inflammation. Curr Mol Med. 2008;8(5):437–45.
15. Radtke FA, Chapman G, Hall J, Syed YA. Modulating neuroinflammation to treat neuropsychiatric disorders. Biomed Res Int. 2017;2017:5071786.
16. Chistyakov DV, Astakhova AA, Sergeeva MG. Resolution of inflammation and mood disorders. Exp Mol Pathol. 2018;105(2):190–201.

17. Schwartz M, Baruch K. The resolution of neuroinflammation in neurodegeneration: leukocyte recruitment via the choroid plexus. EMBO J. 2014;33(1):7–22.
18. Miller GE, Cohen S, Ritchey AK. Chronic psychological stress and the regulation of pro-inflammatory cytokines: a glucocorticoid-resistance model. Health Psychol. 2002;21(6):531–41.
19. Siracusa F, Schaltenberg N, Kumar Y, Lesker TR, Steglich B, Liwinski T, et al. Short-term dietary changes can result in mucosal and systemic immune depression. Nat Immunol. 2023;24(9):1473–86.
20. Xiao R, Ali S, Caligiuri MA, Cao L. Enhancing effects of environmental enrichment on the functions of natural killer cells in mice. Front Immunol. 2021;12:695859.
21. Chabry J, Nicolas S, Cazareth J, Murris E, Guyon A, Glaichenhaus N, et al. Enriched environment decreases microglia and brain macrophages inflammatory phenotypes through adiponectin-dependent mechanisms: Relevance to depressive-like behavior. Brain Behav Immun. 2015;50:275–87.
22. Haykin H, Rolls A. The neuroimmune response during stress: A physiological perspective. Immunity. 2021;54(9):1933–47.
23. Haddad FL, De Oliveira C, Schmid S. Investigating behavioral phenotypes related to autism spectrum disorder in a gene-environment interaction model of Cntnap2 deficiency and Poly I:C maternal immune activation. Front Neurosci. 2023;17:1160243.
24. Atanasova E, Arévalo AP, Graf I, Zhang R, Bockmann J, Lutz A-K, et al. Immune activation during pregnancy exacerbates ASD-related alterations in Shank3-deficient mice. Mol Autism. 2023;14(1):1.
25. Bilbo SD, Block CL, Bolton JL, Hanamsagar R, Tran PK. Beyond infection - Maternal immune activation by environmental factors, microglial development, and relevance for autism spectrum disorders. Exp Neurol. 2018;299(Pt A):241–51.
26. Hsiao EY. Immune dysregulation in autism spectrum disorder. Int Rev Neurobiol. 2013;113:269–302.
27. Chaste P, Leboyer M. Autism risk factors: genes, environment, and gene-environment interactions. Dialogues Clin Neurosci. 2012;14(3):281–92.
28. Montanari M, Balsamo F, Ponterio G, Atiallah IE, Landolfo E, Berretta E, et al. Environmental enrichment ameliorates the impairments of a rodent model of prodromal Parkinson's disease. Brain Behav Immun. 2026;106557.
29. Jurgens HA, Johnson RW. Environmental enrichment attenuates hippocampal neuroinflammation and improves cognitive function during influenza infection. Brain Behav Immun. 2012;26(6):1006–16.
30. Kimura LF, Novaes LS, Picolo G, Munhoz CD, Cheung CW, Camarini R. How environmental enrichment balances out neuroinflammation in chronic pain and comorbid depression and anxiety disorders. Br J Pharmacol. 2022;179(8):1640–60.
31. Vinogradova A, Sysova M, Smirnova P, Sidorova M, Turkin A, Kurilova E, et al. Enriched Environment Induces Sex-Specific Changes in the Adult Neurogenesis, Cytokine and miRNA Expression in Rat Hippocampus. Biomedicines. 2023;11(5).

32. Landolfo E, Cutuli D, Decandia D, Balsamo F, Petrosini L, Gelfo F. Environmental Enrichment Protects against Neurotoxic Effects of Lipopolysaccharide: A Comprehensive Overview. Int J Mol Sci. 2023;24(6).
33. Gelfo F, Mandolesi L, Serra L, Sorrentino G, Caltagirone C. The Neuroprotective Effects of Experience on Cognitive Functions: Evidence from Animal Studies on the Neurobiological Bases of Brain Reserve. Neuroscience. 2018;370:218–35.
34. Tabuchi K, Blundell J, Etherton MR, Hammer RE, Liu X, Powell CM, et al. A neuroligin-3 mutation implicated in autism increases inhibitory synaptic transmission in mice. Science. 2007;318(5847):71–6.
35. Etherton M, Földy C, Sharma M, Tabuchi K, Liu X, Shamloo M, et al. Autism-linked neuroligin-3 R451C mutation differentially alters hippocampal and cortical synaptic function. Proc Natl Acad Sci USA. 2011;108(33):13764–9.
36. Meringolo M, Montanari M, D'Antoni S, Martella G, El Atiallah I, Ponterio G, et al. Impairment of Group I Metabotropic Glutamate Receptors in the Dorsal Striatum of the R451C-Neuroligin 3 Mouse Model of Autism Spectrum Disorder. J Neurochem. 2025;169(10):e70253.
37. Martella G, Meringolo M, Trobiani L, De Jaco A, Pisani A, Bonsi P. The neurobiological bases of autism spectrum disorders: the R451C-neuroligin 3 mutation hampers the expression of long-term synaptic depression in the dorsal striatum. Eur J Neurosci. 2018;47(6):701–8.
38. Rothwell PE, Fuccillo MV, Maxeiner S, Hayton SJ, Gokce O, Lim BK, et al. Autism-associated neuroligin-3 mutations commonly impair striatal circuits to boost repetitive behaviors. Cell. 2014;158(1):198–212.
39. Kooij G, Troletti CD, Leuti A, Norris PC, Riley I, Albanese M, et al. Specialized pro-resolving lipid mediators are differentially altered in peripheral blood of patients with multiple sclerosis and attenuate monocyte and blood-brain barrier dysfunction. Haematologica. 2020;105(8):2056–70.
40. Derada Troletti C, Enzmann G, Chiurchiù V, Kamermans A, Tietz SM, Norris PC, et al. Pro-resolving lipid mediator lipoxin A4 attenuates neuro-inflammation by modulating T cell responses and modifies the spinal cord lipidome. Cell Rep. 2021;35(9):109201.
41. Massaro Cenere M, Tiberi M, Paldino E, D'Addario SL, Federici M, Giacomet C, et al. Systemic inflammation accelerates neurodegeneration in a rat model of Parkinson's disease overexpressing human alpha synuclein. npj Parkinsons Disease. 2024;10(1):213.
42. De Stefano S, Tiberi M, Salvatori I, De Bardi M, Gimenez J, Pirshayan M, et al. Hydrogen sulfide modulates astrocytic toxicity in mouse spinal cord cultures: implications for amyotrophic lateral sclerosis. Antioxidants (Basel). 2024;13(10).
43. Municchi D, Mancini C, Nutarelli S, Tiberi M, D'Addario SL, Chilà G, et al. The oxytocin system mediates behavioral and neurobiological alterations associated with early adversity. Mol Psychiatry. 2025;
44. Krashia P, Cordella A, Nobili A, La Barbera L, Federici M, Leuti A, et al. Blunting neuroinflammation with resolvin D1 prevents early pathology in a rat model of Parkinson's disease. Nat Commun.

2019;10(1):3945.

45. Cutuli D, Caporali P, Gelfo F, Angelucci F, Laricchiuta D, Foti F, et al. Pre-reproductive maternal enrichment influences rat maternal care and offspring developmental trajectories: behavioral performances and neuroplasticity correlates. Front Behav Neurosci. 2015;9:66.
46. Gelfo F, Cutuli D, Foti F, Laricchiuta D, De Bartolo P, Caltagirone C, et al. Enriched environment improves motor function and increases neurotrophins in hemicerebellar lesioned rats. Neurorehabil Neural Repair. 2011;25(3):243–52.
47. Foti F, Laricchiuta D, Cutuli D, De Bartolo P, Gelfo F, Angelucci F, et al. Exposure to an enriched environment accelerates recovery from cerebellar lesion. Cerebellum. 2011;10(1):104–19.
48. Farini D, Cesari E, Weatheritt RJ, La Sala G, Naro C, Pagliarini V, et al. A dynamic splicing program ensures proper synaptic connections in the developing cerebellum. Cell Rep. 2020;31(9):107703.
49. Isingrini E, Camus V, Le Guisquet A-M, Pingaud M, Devers S, Belzung C. Association between repeated unpredictable chronic mild stress (UCMS) procedures with a high fat diet: a model of fluoxetine resistance in mice. PLoS ONE. 2010;5(4):e10404.
50. Angoa-Pérez M, Kane MJ, Briggs DI, Francescutti DM, Kuhn DM. Marble burying and nestlet shredding as tests of repetitive, compulsive-like behaviors in mice. J Vis Exp. 2013;(82):50978.
51. Ellegood J, Crawley JN. Behavioral and neuroanatomical phenotypes in mouse models of autism. Neurotherapeutics. 2015;12(3):521–33.
52. Bonsi P, De Jaco A, Fasano L, Gubellini P. Postsynaptic autism spectrum disorder genes and synaptic dysfunction. Neurobiol Dis. 2022;162:105564.
53. Estes ML, McAllister AK. Immune mediators in the brain and peripheral tissues in autism spectrum disorder. Nat Rev Neurosci. 2015;16(8):469–86.
54. Tomaiuolo P, Piras IS, Sain SB, Picinelli C, Baccarin M, Castronovo P, et al. RNA sequencing of blood from sex- and age-matched discordant siblings supports immune and transcriptional dysregulation in autism spectrum disorder. Sci Rep. 2023;13(1):807.
55. Vacharasin JM, Ward JA, McCord MM, Cox K, Imitola J, Lizarraga SB. Neuroimmune mechanisms in autism etiology - untangling a complex problem using human cellular models. Oxf Open Neurosci. 2024;3:kvae003.
56. Xiong Y, Chen J, Li Y. Microglia and astrocytes underlie neuroinflammation and synaptic susceptibility in autism spectrum disorder. Front Neurosci. 2023;17:1125428.
57. Matta SM, Moore Z, Walker FR, Hill-Yardin EL, Crack PJ. An altered glial phenotype in the NL3R451C mouse model of autism. Sci Rep. 2020;10(1):14492.
58. Suzuki K, Sugihara G, Ouchi Y, Nakamura K, Futatsubashi M, Takebayashi K, et al. Microglial activation in young adults with autism spectrum disorder. JAMA Psychiatry. 2013;70(1):49–58.
59. Than UTT, Nguyen LT, Nguyen PH, Nguyen X-H, Trinh DP, Hoang DH, et al. Inflammatory mediators drive neuroinflammation in autism spectrum disorder and cerebral palsy. Sci Rep. 2023;13(1):22587.

60. Saghazadeh A, Ataeinia B, Keynejad K, Abdolalizadeh A, Hirbod-Mobarakeh A, Rezaei N. A meta-analysis of pro-inflammatory cytokines in autism spectrum disorders: Effects of age, gender, and latitude. J Psychiatr Res. 2019;115:90–102.
61. Eve M, Gandawijaya J, Yang L, Oguro-Ando A. Neuronal cell adhesion molecules may mediate neuroinflammation in autism spectrum disorder. Front Psychiatry. 2022;13:842755.
62. Imbriani P, D'Ambra C, De Mori R, Ionta M, Renna A, Bonsi P. Dysregulation of immune mediators and synaptic plasticity in central nervous system disorders. Cells. 2026;15(2).
63. Wang L, Mirabella VR, Dai R, Su X, Xu R, Jadali A, et al. Analyses of the autism-associated neuroligin-3 R451C mutation in human neurons reveal a gain-of-function synaptic mechanism. Mol Psychiatry. 2024;29(6):1620–35.
64. Sato M, Nakai N, Fujima S, Choe KY, Takumi T. Social circuits and their dysfunction in autism spectrum disorder. Mol Psychiatry. 2023;28(8):3194–206.
65. Soghomonian J-J. The cortico-striatal circuitry in autism-spectrum disorders: a balancing act. Front Cell Neurosci. 2023;17:1329095.
66. Walsh JJ, Christoffel DJ, Heifets BD, Ben-Dor GA, Selimbeyoglu A, Hung LW, et al. 5-HT release in nucleus accumbens rescues social deficits in mouse autism model. Nature. 2018;560(7720):589–94.
67. Chari T, Hernandez A, Couto J, Portera-Cailliau C. A reduced ability to discriminate social from non-social touch at the circuit level may underlie social avoidance in autism. Nat Commun. 2025;16(1):4600.
68. Ponce J, Ulu A, Hanson C, Cameron-Smith E, Bertoni J, Wuebker J, et al. Role of Specialized Pro-resolving Mediators in Reducing Neuroinflammation in Neurodegenerative Disorders. Front Aging Neurosci. 2022;14:780811.
69. Giacobbe J, Benoiton B, Zunszain P, Pariante CM, Borsini A. The Anti-Inflammatory Role of Omega-3 Polyunsaturated Fatty Acids Metabolites in Pre-Clinical Models of Psychiatric, Neurodegenerative, and Neurological Disorders. Front Psychiatry. 2020;11:122.
70. Tiberi M, Chiurchiù V. Specialized Pro-resolving Lipid Mediators and Glial Cells: Emerging Candidates for Brain Homeostasis and Repair. Front Cell Neurosci. 2021;15:673549.
71. Cheadle L. Two's company: Astrocytes and microglia team up to refine developing circuits. Neuron. 2026;114(8):1326–8.
72. Burrows EL, Koyama L, May C, Hill-Yardin EL, Hannan AJ. Environmental enrichment modulates affiliative and aggressive social behaviour in the neuroligin-3 R451C mouse model of autism spectrum disorder. Pharmacol Biochem Behav. 2020;195:172955.
73. Wang C-J, Wu Y, Zhang Q, Yu K-W, Wang Y-Y. An enriched environment promotes synaptic plasticity and cognitive recovery after permanent middle cerebral artery occlusion in mice. Neural Regen Res. 2019;14(3):462–9.
74. Caires CRS, Bossolani-Martins AL. Which form of environmental enrichment is most effective in rodent models of autism? Behav Processes. 2023;211:104915.

75. Ajoolabady A, Kim B, Abdulkhaliq AA, Ren J, Bahijri S, Tuomilehto J, et al. Dual role of microglia in neuroinflammation and neurodegenerative diseases. Neurobiol Dis. 2025;216:107133.

Figures

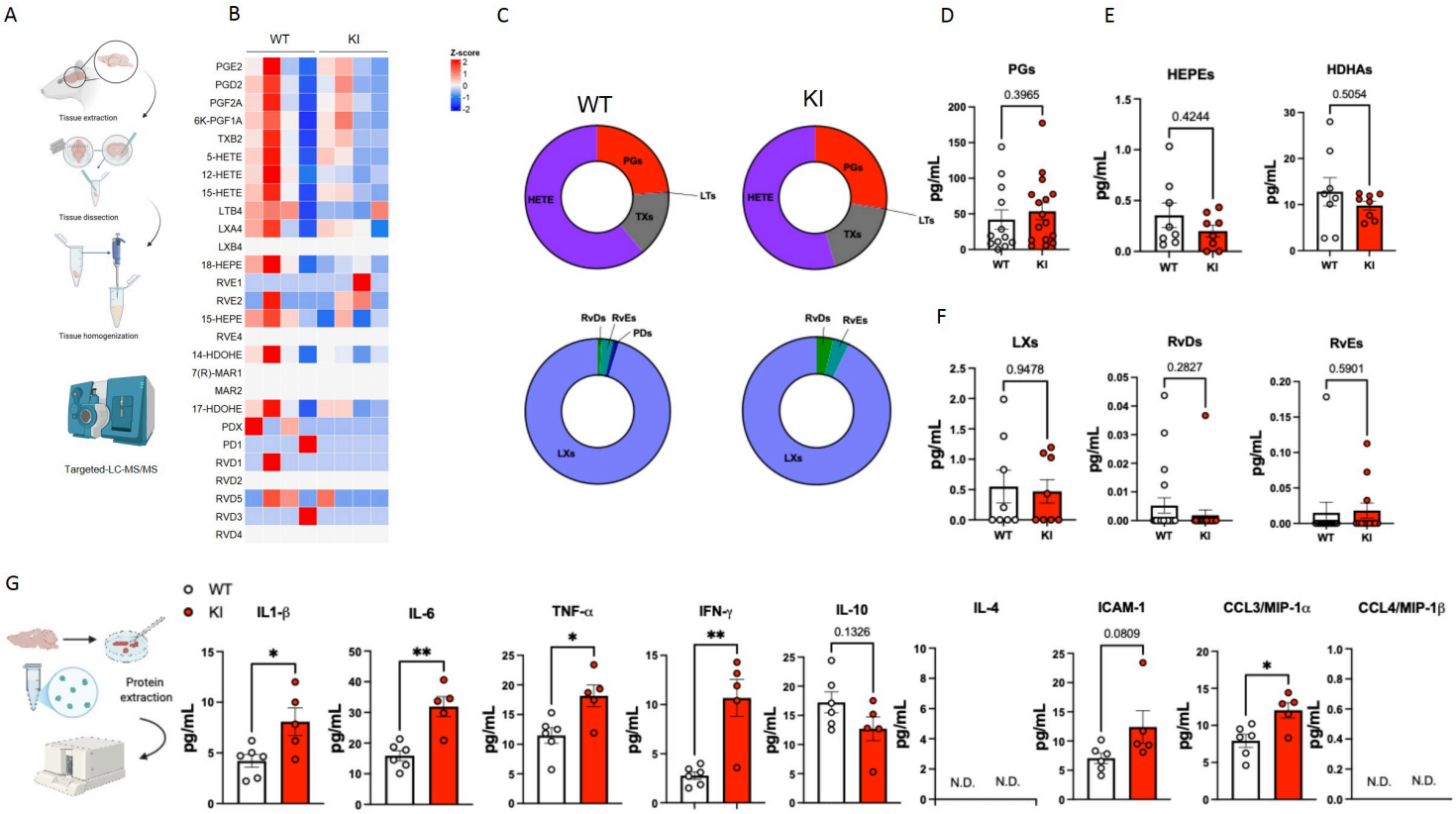


Figure 1

Inflammation-resolution is altered in the striatum of R451C-*Nlgn3* mice. (A)Experimental design for targeted LC-MS/MS in the striatum of WT (n=4) and R451C-*Nlgn3* KI (n=4) mice. (**B,C**) Heatmap and pie charts analyses displaying color-coded changes in Lipid mediators and their main families in WT and KI mice. (**D,F**) Bar graphs showing quantitative changes in key families of lipid mediators. **(G)** Experimental design of multiplex-Luminex assay and bar graphs showing quantitative changes in inflammatory markers, including cytokines, chemokines and adhesion molecules in the striatum of WT (n=6) and KI (n=6) mice. Data are presented as mean ± SEM (pg/mL). Unpaired t-test *p<0.05; **p<0.01.

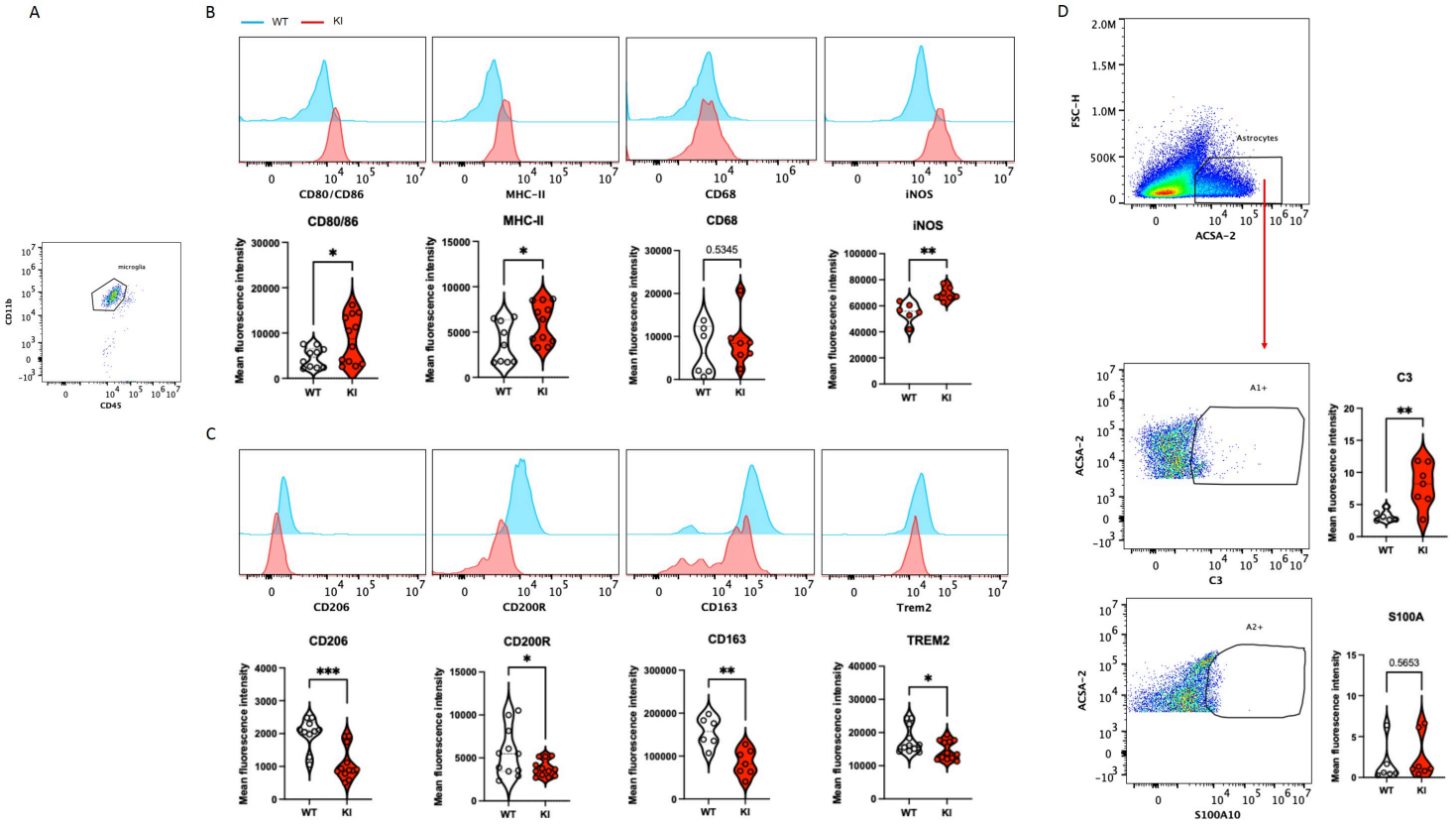


Figure 2

Dysfunction of striatal microglia and astrocytes in R451C-*Nlgn3* mice. (A)Experimental design for tissue dissociation and microglia identification by high dimensional flow cytometry. (**B,C**) Flow cytometry histograms and violin plots displaying changes in (**B**) M1-like (CD80/86, MHC-II, CD68 and iNOS) and (**C**) M2-like (CD206, CD200R, CD163 and Trem2) microglial markers expression in WT (n=6-11) and KI (n =7-12) mice. (**D**) Representative flow cytometry plot for the identification of C3 and S100A10 in ACSA-2+ astrocytes and their quantitative changes shown in violin plots. Data distribution, median and interquartile range are represented. Unpaired t-test *p<0.05; **p<0.01; ***p<0.005.

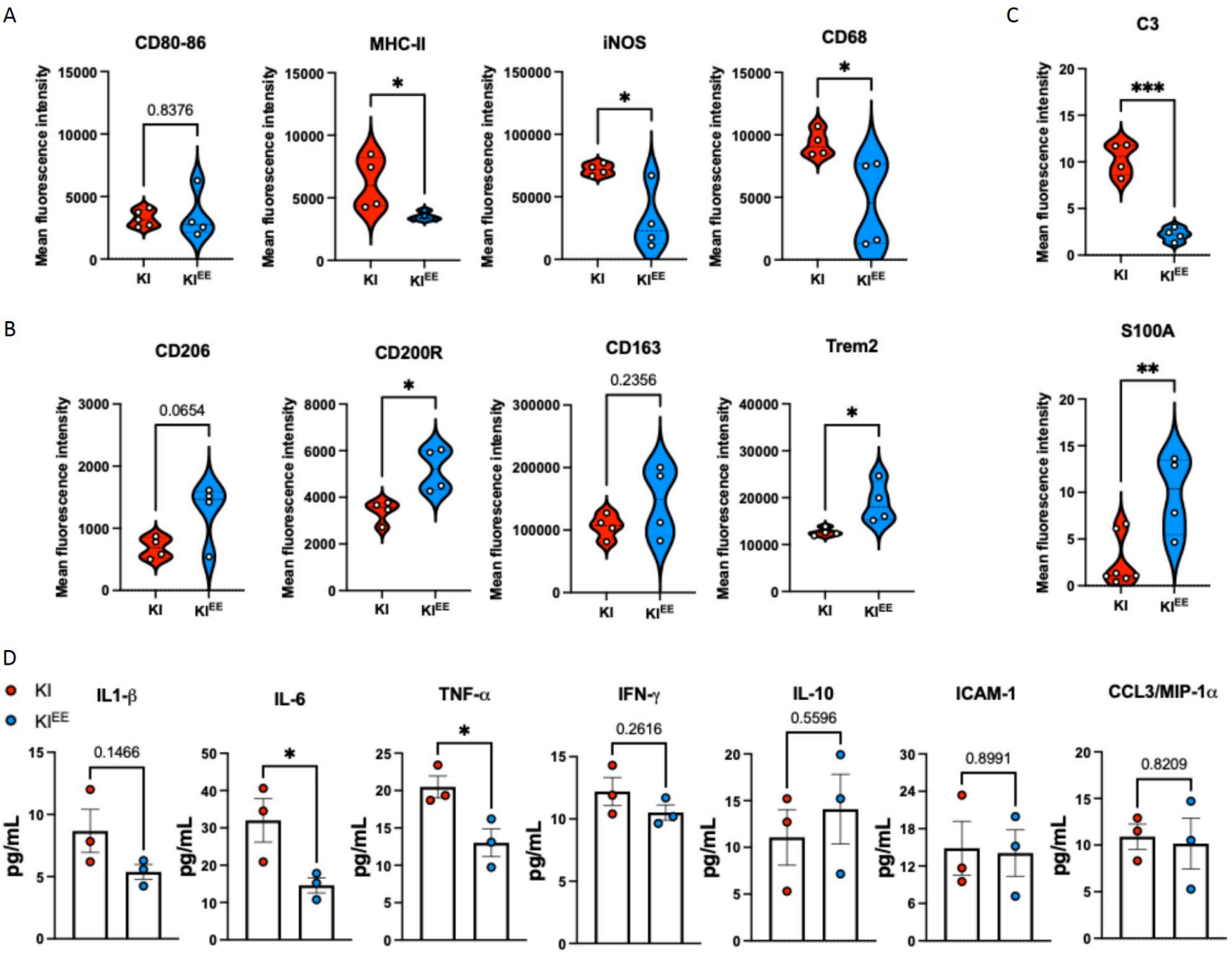


Figure 3

Environmental enrichment reverses the inflammatory milieu in the R451C-*Nlgn3* striatum. The violin plots report the striatal expression of (**A**) M1-like (CD80/86, MHC-II, CD68 and iNOS) and (**B**) M2-like (CD206, CD200R, CD163 and Trem2) microglial markers, or (**C**) C3 and S100A10 expression in ACSA-2+ astrocytes of R451C-*Nlgn3* mice reared in standard (KI) or EE (KI^{EE}) conditions. Data distribution, median and interquartile range are represented. Unpaired t-test *p<0.05; **p<0.01; ***p<0.005. (**D**) Bar graphs showing quantitative changes in inflammatory markers, including cytokines, chemokines and adhesion molecules, in the striatum of R451C-*Nlgn3* mice reared in standard (KI) or EE (KI^{EE}) conditions. Data are presented as mean ± SEM. Unpaired t-test *p<0.05.

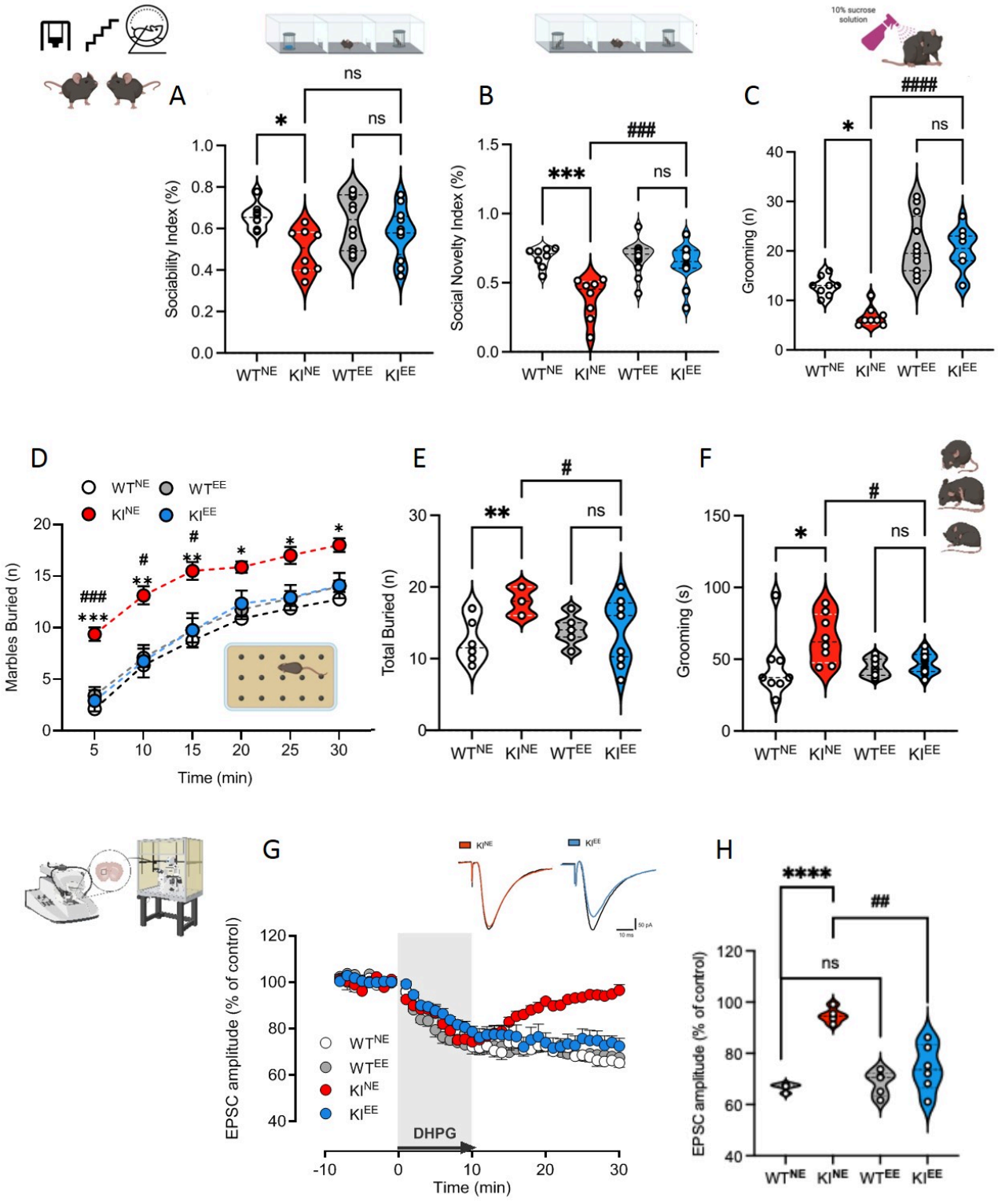


Figure 4

Behavioral and synaptic alterations are rescued by environmental enrichment. The violin plots show the effect of EE on the (**A**) sociability index ($F(1,36)=0.55$, $p=0.462$), during the sociability phase, and (**B**) social novelty index ($F(1,36)=9.35$, $p=0.004$), during the social novelty phase, in the Three-chamber test. (**C**) Violin plots reporting the number of self-grooming events recorded during the Splash test ($F(1,36)=62.04$, $p<0.0001$). (**D,E,F**) The plots report the effects of EE in the Marble burying test. (**D**) Effect

of EE on the time-course of marbles buried (F(3,36)=6.760, p=0.0010). For clarity, the significance in the Bonferroni's multiple comparisons post-hoc test is shown only for the WT^{NE} vs KI^{NE} (*) and KI^{EE} vs KI^{NE} (#) comparisons. (**E**) Effect of EE on the total number of marbles buried (F(1,36)=1. 848, p=0.182), and (**F**) on the time spent grooming (F(1,36)=4.242, p=0.047) during the test. For the experiments shown in (**A-F**) statistical significance was determined by a 2-way ANOVA with Bonferroni's multiple comparisons test (* for inter-genotype and # for intra-genotype comparisons). (**G,H**) The graphs report the results of patch-clamp electrophysiology recordings of excitatory postsynaptic currents (EPSCs) from striatal slices obtained from 3 WT^{NE}, 4 KI^{NE}, 4 WT^{EE}, and 4 KI^{EE} mice. EPSC amplitude is expressed as % of baseline pre-DHPG mean value. (**G**) Time-course of the EPSC amplitude recorded before, during, and after DHPG application to induce LTD (50 µM, 10 min). Data are presented as mean ± SEM. (**H**) The violin plot summarizes the mean amplitude of EPSCs measured during the last 5 minutes of recording. Statistical significance (* for inter-genotype and # for intra-genotype comparisons) was determined by unpaired t-test: WT^{NE} vs KI^{NE}, ****p<0.0001; WT^{NE} vs WT^{EE}, p=0.539; KI^{NE} vs KI^{EE}, $^{\#\#}$p=0.001; WT^{EE} vs KI^{EE}, p=0.243.

Supplementary Files

This is a list of supplementary files associated with this preprint. Click to download.

- SupplementaryFigure1.jpg
- SupplementaryFigure2.jpg
- SupplementaryFigure3.jpg
- SupplementaryTable1.docx